THE JOURNAL OF BIOLOGICAL CHEMISTRY
Vol. 280, No. 21, Issue of May 27, pp. 20762–20774, 2005

Printed in U.S.A.

Crystal Structures of Undecaprenyl Pyrophosphate Synthase in Complex with Magnesium, Isopentenyl Pyrophosphate, and Farnesyl Thiopyrophosphate

ROLES OF THE METAL ION AND CONSERVED RESIDUES IN CATALYSIS*[S]

Received for publication, February 24, 2005
Published, JBC Papers in Press, March 23, 2005, DOI 10.1074/jbc.M502121200

Rey-Ting Guo‡§¶‖, Tzu-Ping Ko¶‖, Annie P.-C. Chen§¶, Chih-Jung Kuo¶, Andrew H.-J. Wang‡§¶, and Po-Huang Liang‡§¶‡‡**

From the ‡Taiwan International Graduate Program, Academia Sinica, Taipei 115, Taiwan, the ¶Institute of Biological Chemistry, Academia Sinica, Taipei 115, Taiwan, and the §Institute of Biochemical Sciences, National Taiwan University, Taipei 106, Taiwan

Undecaprenyl pyrophosphate synthase (UPPs) catalyzes the consecutive condensation reactions of a farnesyl pyrophosphate (FPP) with eight isopentenyl pyrophosphates (IPP), in which new *cis*-double bonds are formed, to generate undecaprenyl pyrophosphate that serves as a lipid carrier for peptidoglycan synthesis of bacterial cell wall. The structures of *Escherichia coli* UPPs were determined previously in an orthorhombic crystal form as an apoenzyme, in complex with Mg^{2+}/sulfate/Triton, and with bound FPP. In a further search of its catalytic mechanism, the wild-type UPPs and the D26A mutant are crystallized in a new trigonal unit cell with Mg^{2+}/IPP/farnesyl thiopyrophosphate (an FPP analogue) bound to the active site. In the wild-type enzyme, Mg^{2+} is coordinated by the pyrophosphate of farnesyl thiopyrophosphate, the carboxylate of Asp^{26}, and three water molecules. In the mutant enzyme, it is bound to the pyrophosphate of IPP. The [Mg^{2+}] dependence of the catalytic rate by UPPs shows that the activity is maximal at [Mg^{2+}] = 1 mM but drops significantly when Mg^{2+} ions are in excess (50 mM). Without Mg^{2+}, IPP binds to UPPs only at high concentration. Mutation of Asp^{26} to other charged amino acids results in significant decrease of the UPPs activity. The role of Asp^{26} is probably to assist the migration of Mg^{2+} from IPP to FPP and thus initiate the condensation reaction by ionization of the pyrophosphate group from FPP. Other conserved residues, including His^{43}, Ser^{71}, Asn^{74}, and Arg^{77}, may serve as general acid/base and pyrophosphate carrier. Our results here improve the understanding of the UPPs enzyme reaction significantly.

Isoprenoids are an extensive group of natural products consisting of five-carbon isopentenyl units (1, 2). A class of enzymes involved in the biosynthesis of the linear isoprenoid polymers each catalyzes consecutive 1′–4 condensation reactions of a designated number of isopentenyl pyrophosphate (IPP)[1] with a single farnesyl pyrophosphate (FPP) (3). These prenyltransferases are classified as *cis*- and *trans*-isoprenyl pyrophosphate synthases according to the stereochemical outcome of their products resulted from IPP condensation (4). The enzymatic products play essential biological roles; for example, the *trans*-C_{40} octaprenyl pyrophosphate (OPP) synthesized by *trans*-type OPP synthase constitutes the side chain of ubiquinone (5, 6), and the C_{55} undecaprenyl pyrophosphate (UPP) synthesized by *cis*-type UPPs serves as a lipid carrier for bacterial peptidoglycan biosynthesis (7, 8). *Cis*- and *trans*-prenyltransferases apparently utilize different strategies for substrate binding and catalysis while sharing the same allylic substrate FPP and homoallylic substrate IPP. This was initially supported by the lack of sequence similarity between the two groups of prenyltransferases (9, 10) and was further validated unequivocally by the crystal structures of both OPP synthase and UPPs (11–16). The *trans*-type enzymes involve a mechanism of ionization, condensation and elimination reactions, which are initiated by breaking the bond between the pyrophosphate and the farnesyl group, followed by electrophilic attack of the C1 carbonium of the farnesyl on the C4 of IPP, and concluded with elimination of the proton on C2 of IPP (17). The elimination of the pyrophosphate group of FPP is facilitated by the Mg^{2+} that is coordinated to the DD*XX*D motif conserved in all the *trans*-prenyltransferases (18–20).

The reaction mechanism for catalysis of the *cis*-type enzymes is less understood. In the *cis*-type UPPs, no DD*XX*D motif was found, and our previous fluorescence binding study showed that FPP binding did not require Mg^{2+}, whereas IPP binding and the ensuing reactions absolutely required the metal ion (21). Based on the crystal structure of UPPs in complex with FPP, the pyrophosphate head group of FPP was bound to the backbone N atoms of Gly^{29} and Arg^{30} as well as the side chains of Asn^{28}, Arg^{30}, and Arg^{39} through hydrogen bonds (16). No Mg^{2+} was found associated with the pyrophosphate group of FPP in this crystal structure. IPP did not co-crystallize with UPPs and was suspected to bind in the active site via hydrogen

* This work was supported by grants from Academia Sinica and from National Science Council (NSC91-3112-P-001-019-Y (to A. H.-J. W.) and NSC92-2113-M-001-026 (to P.-H. L.). The National Synchrotron Radiation Research Center, Taiwan, is supported by the National Science Council of Taiwan.The costs of publication of this article were defrayed in part by the payment of page charges. This article must therefore be hereby marked "*advertisement*" in accordance with 18 U.S.C. Section 1734 solely to indicate this fact.

The atomic coordinates and structure factors (code 1X06, 1X08, 1X07, and 1X09) have been deposited in the Protein Data Bank, Research Collaboratory for Structural Bioinformatics, Rutgers University, New Brunswick, NJ (http://www.rcsb.org/).

[S] The on-line version of this article (available at http://www.jbc.org) contains two additional figures.

‖ These two authors contributed equally to this work.

** To whom correspondence may be addressed. Tel.: 886-2-2788-1981; Fax: 886-2-2788-2043; E-mail: ahjwang@gate.sinica.edu.tw.

‡‡ To whom correspondence may be addressed. Tel.: 886-2-2785-5696 (ext. 6070); Fax: 886-2-2788-9759; E-mail: phliang@gate.sinica.edu.tw.

[1] The abbreviations used are: IPP, isopentenyl pyrophosphate(s); FPP, farnesyl pyrophosphate(s); OPP, octaprenyl pyrophosphate; UPP, undecaprenyl pyrophosphate; UPPs, undecaprenyl pyrophosphate synthase; FsPP, farnesyl thiopyrophosphate.

bonds to Arg^{194} and Arg^{200} (16). The hydrocarbon moiety of FPP was in contact with several hydrophobic amino acids, among which Leu^{85}, Leu^{88}, and Phe^{89} were located in the helix α_3 that reoriented for better UPPs-FPP interaction. A loop containing amino acids 72–82 was responsible for the conformational change (22). This region was highly flexible, and its electron density was invisible in the apo-UPPs structure (13, 14), but it could be seen when the enzyme was complexed with Triton or FPP (15, 16).

In the present study, we determine four crystal structures of the wild-type UPPs and the mutant D26A in complex with Mg^{2+}, IPP, and farnesyl thiopyrophosphate (FsPP), an FPP analogue that we synthesized previously (21). In FsPP, the bridging oxygen atom between the farnesyl and the pyrophosphate group is replaced with a sulfur atom to make the ionization reaction much slower. These new ternary structures are at higher resolution than that of the UPPs-FPP binary complex and provide detailed molecular contacts of the two substrates FsPP and IPP with the enzyme. In addition, a Mg^{2+} is octahedrally coordinated by the pyrophosphate of either FsPP or IPP, the carboxylate of Asp^{26} and/or water molecules. With both substrates bound, the flexible loop of 72–82 is now clearly visible, providing information about the conformational change as required for catalysis. We further perform fluorescence binding experiments to probe this substrate-binding mode. The relationship between the enzyme activity and Mg^{2+} concentration is examined to investigate the role of the metal ion in catalysis. The binding constant of Mg^{2+} is then determined. Finally, the essential Asp^{26} is replaced by other charged amino acids to investigate their effects on the enzyme, which turns out to be inactivated. These observations allow us to gain fuller understanding on the reaction mechanism of UPPs.

EXPERIMENTAL PROCEDURES

Materials—Radiolabeled [^{14}C]IPP (55 mCi/mmol) was purchased from Amersham Biosciences. FPP and IPP were obtained from Sigma. *PfuTurbo* DNA polymerase was obtained from Invitrogen. The plasmid minipreparation kit, DNA gel extraction kit, and Ni^{2+}-nitrilotriacetic acid resin were purchased from Qiagen. Potato acid phosphatase (2 units/mg) was purchased from Roche Applied Science. FXa and the protein expression kit (including the pET32Xa/Lic vector and competent JM109 and BL21 (DE3) cells) were obtained from Novagen. The QuikChange site-directed mutagenesis kit was obtained from Stratagene. All commercial buffers and reagents were of the highest grade. The UPPs wild type and D26A mutant for crystallization were prepared using the reported procedure (23, 24).

Crystallization and Data Collection—Wild-type and D26A UPPs-substrate mixture solutions contained 2.5 mM $MgCl_2$ and 2.5 mM IPP were prepared by mixing the UPPs solutions (10 mg/ml in 25 mM Tris-HCl, 150 mM NaCl, 0.03% Triton X-100, pH 7.5) with dried $MgCl_2$ and IPP powder. Wild-type and D26A UPPs in complex with Mg^{2+} and IPP were crystallized using the hanging drop method from Hampton Research (Laguna Niguel, CA) by mixing 2 μl of the mixture solution with 2 μl of the mother liquor (20% ethylene glycol and 2–5% PEG 35,000), equilibrating with 500 μl of the mother liquor at room temperature. Within 2 days, crystals grew to dimensions of about 0.3 × 0.3 × 0.2 mm, and then the crystals were soaked with a cryoprotectant solution of 2.5 mM $MgCl_2$, 2.5 mM IPP, 30% ethylene glycol, and 5% PEG 35,000 for 1 day. Crystals of wild-type and D26A UPPs in complex with Mg^{2+}, IPP, and FsPP were obtained by soaking the previously grown crystals with cryoprotectant solution that contains IPP and FsPP (2.5 mM $MgCl_2$, 2.5 mM IPP, 2.5 mM FsPP, 30% ethylene glycol, and 5% PEG 35,000) for 1 day.

Data for crystals of the wild-type and D26A UPPs in complex with Mg^{2+}, IPP, and FsPP and the crystal of D26A in complex with Mg^{2+} and IPP were collected at beam line BL17B2 of the National Synchrotron Radiation Research Center (NSRRC, Hsinchu, Taiwan). Data for the wild-type UPPs crystal in complex with Mg^{2+} and IPP were collected in house using a Rigaku MicroMax002 x-ray generator equipped with an R-Axis IV^{++} image plate detector. The diffraction data were processed using the programs of HKL and HKL2000 (25). Statistics for the four data sets are listed in Table I. Prior to use in structural refinements, 5% randomly selected reflections were set aside for calculating R_{free} as a monitor (26).

Structure Determination and Refinement—The crystal structures of the wild-type UPPs and the D26A mutant in complex with FsPP and IPP were determined by the molecular replacement method using the CNS program (27). The trigonal crystals of space group $P3_x21$ contained one UPPs monomer in an asymmetric unit, and the molecular 2-fold axis of the dimer must be in coincidence with one of the crystallographic dyad axes. The models of Protein Data Bank 1JP3, 1UEH, and 1V7U were used as search models, and the monomer A of 1V7U containing bound FPP (16) yielded the best solution for the wild-type crystal in complex with Mg^{2+}, FsPP, and IPP. The space group was determined as $P3_221$. With all solvent and cofactor molecules removed, the model yielded an initial R value of 0.39 using all positive reflections at 1.9-Å resolution upon rigid body refinement.

The $2F_o - F_c$ difference Fourier map showed clear electron densities for most amino acid residues including the catalytic loop of 72–82, whereas the N- and C-terminal segments were still disordered. Densities for the FsPP were clear, and a geranyl fragment was also observed in the tunnel. Those for the IPP molecule were weak and can only be modeled as a phosphate ion. Subsequent refinement with incorporation of a $Mg^{2+}(H_2O)_3$ ion and 330 water molecules according to a 1.0 σ map level yielded R and R_{free} values of 0.183 and 0.231, respectively, at 1.9-Å resolution. The other three crystals are all isomorphous to the first one. Direct use of the previous model gave initial R values of 0.26–0.30 upon rigid body refinement against the new data sets. By employing similar procedures, these crystal structures were refined with the addition of cofactors and solvent molecules. Statistics for the final models are listed in Table I.

All manual modifications of the models were performed on an SGI Fuel computer using the program O (28). Computational refinements, which included maximal likelihood and simulated annealing protocols, were carried out using CNS. The programs Alscript (29), MolScript (30), BobScript (31), and Raster3D (32) were used in producing figures.

Fluorescence Binding Experiments—The fluorescence emission spectra of 1 μM wild-type or D26A mutant UPPs with different ligands were measured in a buffer of 50 mM KCl and 100 mM Hepes (pH 7.5). The enzyme solutions used in the fluorescence study were first dialyzed in the buffer with the addition of 1 mM EDTA to remove any metal ion possibly bound to the UPPs, and then dialyzed against the buffer to remove EDTA. The samples were excited at 285 nm, and the emission spectra from 300 to 450 nm were recorded using a F-4500 fluorescence spectrophotometer (Hitachi, Japan). The fluorescence spectra with the addition of 4 μM FsPP to the enzyme and the mixture with the further addition of 20 μM IPP in the presence of 1 or 50 mM Mg^{2+} or absence of Mg^{2+} were measured. Furthermore, in the absence of FsPP, a high concentration of IPP (1 mM) was added to wild-type or D26A mutant UPPs, and the fluorescence spectra were recorded.

Reaction Kinetics of UPPs with Various Concentrations of Mg^{2+}—The purified UPPs was dialyzed twice in a 2-liter solution of 25 mM Tris (pH 7.5), 50 mM KCl, and 1 mM EDTA to remove any Mg^{2+} possibly associated with the enzyme. After dialysis, different concentrations of Mg^{2+} were added back to the solution, and the kinetic parameters were measured. In the K_m measurements of MgIPP under $[Mg^{2+}] < 1$ mM, the [MgIPP] was calculated based on the reported $K_{d(MgIPP)} = 520$ μM in solution (33). When $[Mg^{2+}]$ was in excess, the Mg^{2+} ion became competitively inhibitory, and its inhibition constant was calculated using Equation 1.

$$1/V = K_m/V_m(1 + [I]/K_i)1/[S] + 1/V_m \quad \text{(Eq. 1)}$$

In this equation, K_m is the Michaelis constant of the substrate MgIPP; K_i is the inhibition constant of free Mg^{2+}; V_m is the maximal velocity; and [I] and [S] represent the $[Mg^{2+}]$ and [MgIPP] in the reaction mixture, respectively. Measurements of the initial rate (V) employed our procedure in the presence of 0.1% Triton to facilitate product release (23).

Site-directed Mutagenesis of UPPs—UPPs mutants were prepared by using QuikChange site-directed mutagenesis kit in conjunction with the *Escherichia coli* UPPs gene template in the pET32Xa/Lic vector. The mutagenic primer oligonucleotides for performing site-directed mutagenesis were prepared by Biobasic Inc. (Canada), and the sequences were 5′-CGTCATGTTGCGATCATTATGGAAGGCAATGGTCGCTGGGCA-3′ for D26E, 5′-CGTCATGTTGCGATCATTATGAAAGGCAATGGTCGCTGGGCA-3′ for D26K, and 5′-CGTCATGTTGCGATCATTATGCGCGGCAATGGTCGCTGGGCA-3′ for D26R. The basic procedure of mutagenesis utilizes a supercoiled double-stranded DNA vector with an insert of interest and two synthetic oligonucleotide primers containing

TABLE I
Data collection and refinement statistics for the trigonal UPPs crystals

Crystals	Wild type + FsPP + IPP (WTF)	Wild type + IPP (WTI)	D26A + FsPP + IPP (MTF)	D26A + IPP (MTI)
Data collection				
Space group	$P3_221$	$P3_221$	$P3_221$	$P3_221$
Resolution (Å)[a]	25 to 1.9 (1.97 to 1.90)	50 to 2.2 (2.28 to 2.20)	25 to 1.9 (1.97 to 1.90)	25 to 1.87 (1.94 to 1.87)
Unit cell dimensions				
a, *b* (Å)	58.12	57.79	57.71	57.30
c (Å)	118.94	119.13	118.99	118.43
No. of reflections observed	78,391 (4788)	56,384 (3735)	70,762 (4239)	74,103 (3500)
Unique	19,022 (1778)	12,171 (1130)	18,754 (1656)	18,959 (1537)
Completeness (%)	98.9 (95.0)	99.0 (93.3)	98.7 (89.3)	97.0 (80.6)
R_{merge} (%)	7.2 (39.4)	6.5 (40.2)	6.9 (40.3)	6.5 (30.7)
$I/\sigma(I)$	19.9 (2.4)	24.4 (3.3)	18.6 (2.1)	22.7 (2.3)
Refinement				
No. of reflections[b]	17,974 (1557)	11,617 (984)	17,690 (1465)	17,841 (1345)
R_{work} (%)	18.2 (25.1)	18.4 (26.1)	17.3 (26.7)	17.6 (27.3)
R_{free} (%)	23.4 (28.8)	25.3 (32.5)	21.9 (32.6)	21.5 (34.2)
Geometry deviations				
Bond lengths (Å)	0.018	0.018	0.019	0.019
Bond angles (°)	1.8	1.8	1.7	1.8
No. of all non-hydrogen atoms	2200	2058	2185	2146
Mean *B* values (Å^2)	28.4	33.4	26.7	30.1
No. of water molecules	330	193	331	280
Mean *B* values (Å^2)	46.8	45.3	43.4	49.0
Ramachandran plot (%)				
Most favored	91.7	92.3	93.1	93.7
Additionally allowed	8.3	7.7	6.9	6.3

[a] Values in the parentheses are for the highest resolution shells.
[b] All positive reflections are used in the refinements.

the desired mutation. The mutation was confirmed by sequencing the entire UPPs mutant gene of the plasmid obtained from overnight culture. The correct construct was subsequently transformed to *E. coli* BL21 (DE3) for protein expression. The procedure for protein purification followed our reported protocol (23). Each purified mutant UPPs was verified by mass spectroscopic analysis, and its purity (>95%) was checked by SDS-PAGE.

Kinetic Parameters for UPPs Mutants—For enzyme activity measurements, mutant UPPs enzymes (0.1 μM D26E, D26K, and D26R) were used. The reaction was initiated in a 200-μl solution containing 100 mM Hepes (pH 7.5), 50 mM KCl, 0.5 mM $MgCl_2$, and 0.1% Triton X-100. For FPP K_m, FPP concentrations were ranged from 0.2 to 10 μM, whereas IPP was 75 μM. For IPP K_m, IPP concentrations were ranged from 2 to 500 μM, whereas FPP was 10 μM. The reaction mixtures were withdrawn at intervals of 3 h at 25 °C. The reaction was terminated by adding 10 mM (final concentration) EDTA, and the product was extracted with 1-butanol. The product was then quantitated by counting the radioactivity in the butanol phase ([^{14}C]IPP remained in the aqueous phase) using a Beckman LS6500 scintillation counter. Each UPPs mutant's steady-state k_{cat} was calculated based on the rate of IPP consumption.

RESULTS

Overall Structures and Comparison—IPP can serve as an allylic substrate, although with poor activity, to react with another IPP under the catalysis of UPPs (34). In this study, besides soaking UPPs with FsPP and IPP to form a ternary complex, we also soaked UPPs with IPP only and found IPP in both FPP and IPP sites. Since Asp^{26} plays an essential role in catalysis, we further determine the D26A mutant crystal structures with these substrate and analogue. Four new crystal structures are presented here, which correspond to (i) the wild-type UPPs complexed with FsPP, IPP, and Mg^{2+} (denoted WTF), (ii) the wild-type UPPs complexed with two IPP (one in the FPP site and another in the IPP site) and Mg^{2+} (WTI), (iii) the D26A mutant complexed with FsPP, IPP, and Mg^{2+} (MTF), and (iv) the D26A mutant complexed with two IPP and Mg^{2+} (MTI). FsPP is an almost inactive thiol analogue of FPP, and therefore it can be co-crystallized with IPP without forming a product (21). The refined models in this new trigonal crystal form contain continuous polypeptide chains starting at residues 9–13 and terminating at 239–240 (Table II).

These new trigonal crystals contain one UPPs monomer as an asymmetric unit, and the functional dimer is formed with another dyad-related monomer. The protein folds of WTF, WTI, MTF, and MTI are identical to each other and similar to those observed in the orthorhombic crystals (14–16), comprising a central β-sheet with six parallel strands and seven surrounding α-helices (Fig. 1). In addition, five regions are identified as 3_{10}-helices, including 71–77, 112–116, 168–172, 205–209, and 220–224. The first 3_{10}-helix contains two consecutive turns. It corresponds to a major part of the flexible loop in the apoenzyme and can only be seen with bound substrate molecules. This loop is responsible for the interchange of open (apoenzyme and product-bound) and closed (substrate-bound) protein conformations as proposed previously (22). In the new structures with both allylic and homoallylic sites occupied, the loop becomes significantly more visible, as reflected by the clear electron density map in this region (Supplementary Fig. 1).

The protein conformations of the four refined UPPs models resemble the closed conformation with bound FPP (16), with a slight variation in helix α_2, but these structures still contain interesting different features relevant to the catalysis using Mg^{2+} (see below). The root mean square deviations among the four structures are 0.22–0.45 Å for 223–228 Cα atoms. These models superimpose with our previously solved apo-UPPs (Protein Data Bank code 1JP3), the UPPs-Triton complex (1UEH) and the UPPs-FPP complex (1V7U) structures by root mean square deviations of 1.24–1.39, 1.73–1.82, and 0.73–0.95 Å, respectively, for all equivalent 210–224 Cα atoms. Superposition is best in general only for the six β-strands and the three helices α_5, α_6, and α_7, with the largest differences between the current models (most closed) and the Triton-bound model (most open), where the helix α_3 deviates at the N terminus by 7.7–8.5 Å, as shown in Fig. 2*A*. This helix is kinked in all UPPs structures, whereas the precise kink point varies, and the small and large kink angles determine the open and closed conformations of the enzyme, as shown in Fig. 2*B*. Helices α_1 and α_2 also show large deviations of 2.9–4.2 Å between these different conformations. Interestingly, the FPP-bound UPPs

TABLE II
Summary of the UPPs structures with bound cofactors

Models containing Triton and FPP correspond to PDB entries 1UEH (chain B) and 1V7U (chain A), respectively. The numbers in parentheses are for the average *B* values in Å^2.

	Triton	FPP	WTF	WTI	MTF	MTI
Conformation	Open	Closed	Closed	Closed	Closed	Closed
Polypeptide	17–241 (21.2)	13–239 (32.2)	12–240 (25.0)	10–240 (32.0)	13–240 (23.8)	9–239 (27.0)
Active site (S1)	SO_4 (24.9)	FPP (59.4)	FsPP (34.9)	IPP (38.5)	FsPP (22.1)	PP_i (47.3)
Active site (S2)	SO_4 (44.6)		PO_4 (50.1)	PO_4 (46.7)	C_5 (22.8)	IPP (47.8)
Active site (M)			$Mg(H_2O)_3$ (27.7)	$Mg(H_2O)_3$ (27.8)		$Mg(H_2O)_4$ (48.6)
Distal FPP site	Triton (18.5)	FPP (53.2)	C_{10} (34.1)		C_{10} (33.2)	

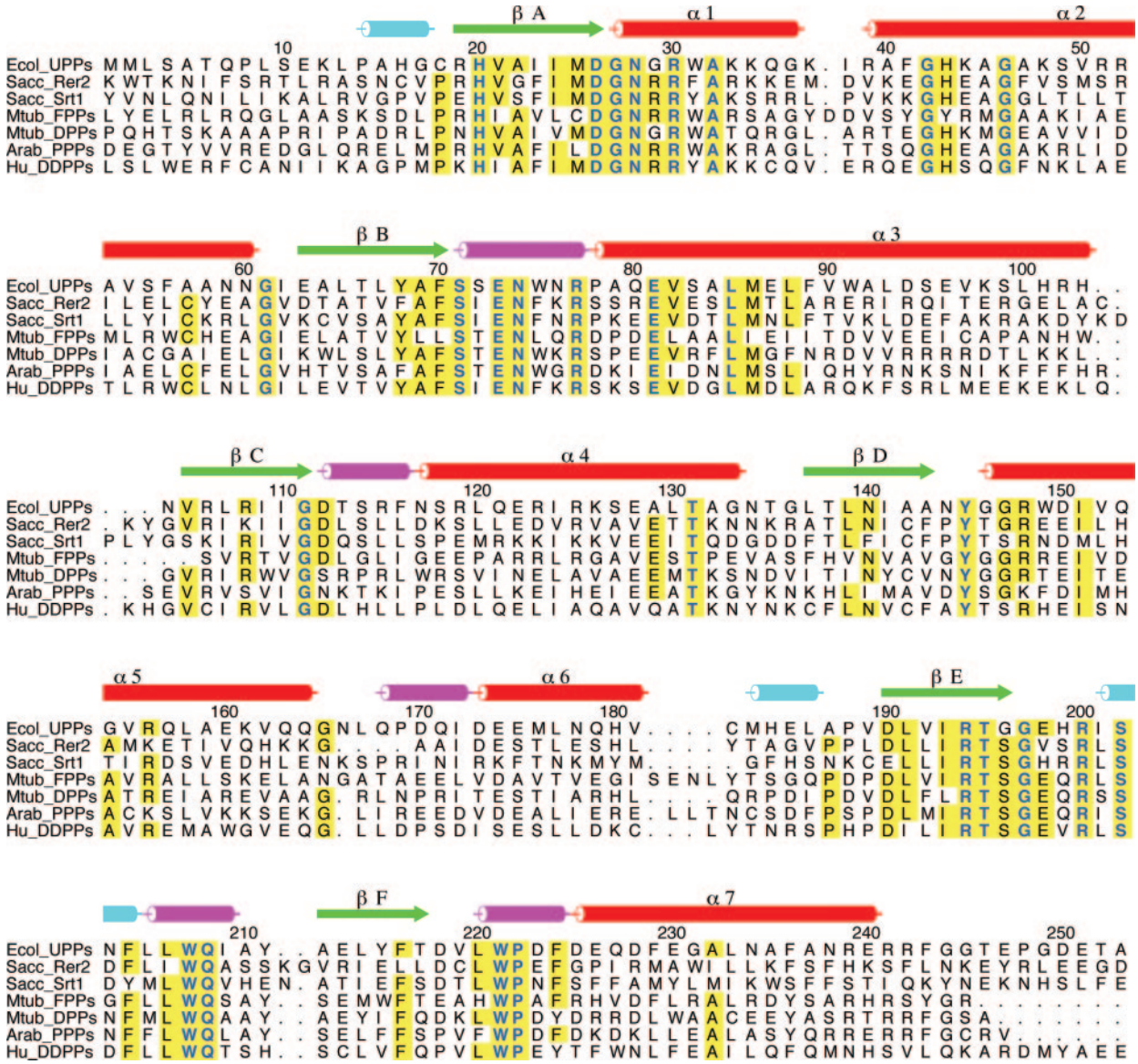

FIG. 1. **Sequence alignment of *cis*-prenyl transferases.** The complete amino acid sequence of *E. coli* UPPs (residues 1–253) is aligned with corresponding partial sequences of yeast dehydrodolichyl pyrophosphate synthase (*DDPPs*) Rer2, yeast dehydrodolichyl pyrophosphate synthase Srt1, *Mycobacterium tuberculosis* farnesyl pyrophosphate synthase Rv1086, *M. tuberculosis* decaprenyl pyrophosphate synthase Rv2361c, *Arabidopsis thaliana* polyprenyl pyrophosphate synthase, and human DDPPs. The numbers and secondary structure elements shown *above* the sequences are for the *E. coli* UPPs and based on analysis of its crystal structure. The *green arrows* denote the locations of β-strands, and the *red*, *magenta*, and *cyan cylinders* are for the α-helices, 3_{10}-helices, and turns, respectively. Amino acids with at least five identities in the seven sequences are *shaded* in *yellow*, and the strictly conserved residues are *highlighted* in *blue*.

(1V7U) has similar dispositions of the helices α_1 and α_2 as those in the Triton-bound structure (1UEH) and thus is a little more open than the structures studied here with bound Mg^{2+} and two anionic substrates. The change from open to closed conformation is probably triggered by interactions with the substrate molecules (see below).

There are two sulfate ions bound to the active site of the UPPs-Triton complex. In the previous UPPs-FPP complex, only one site (*S1* in Fig. 2*A*) is occupied, although two FPP molecules are bound to a UPPs monomer. Both of the sulfate ions are now replaced with real pyrophosphate substrate molecules, and the assignments of S1 and S2 sites for binding FPP and IPP are

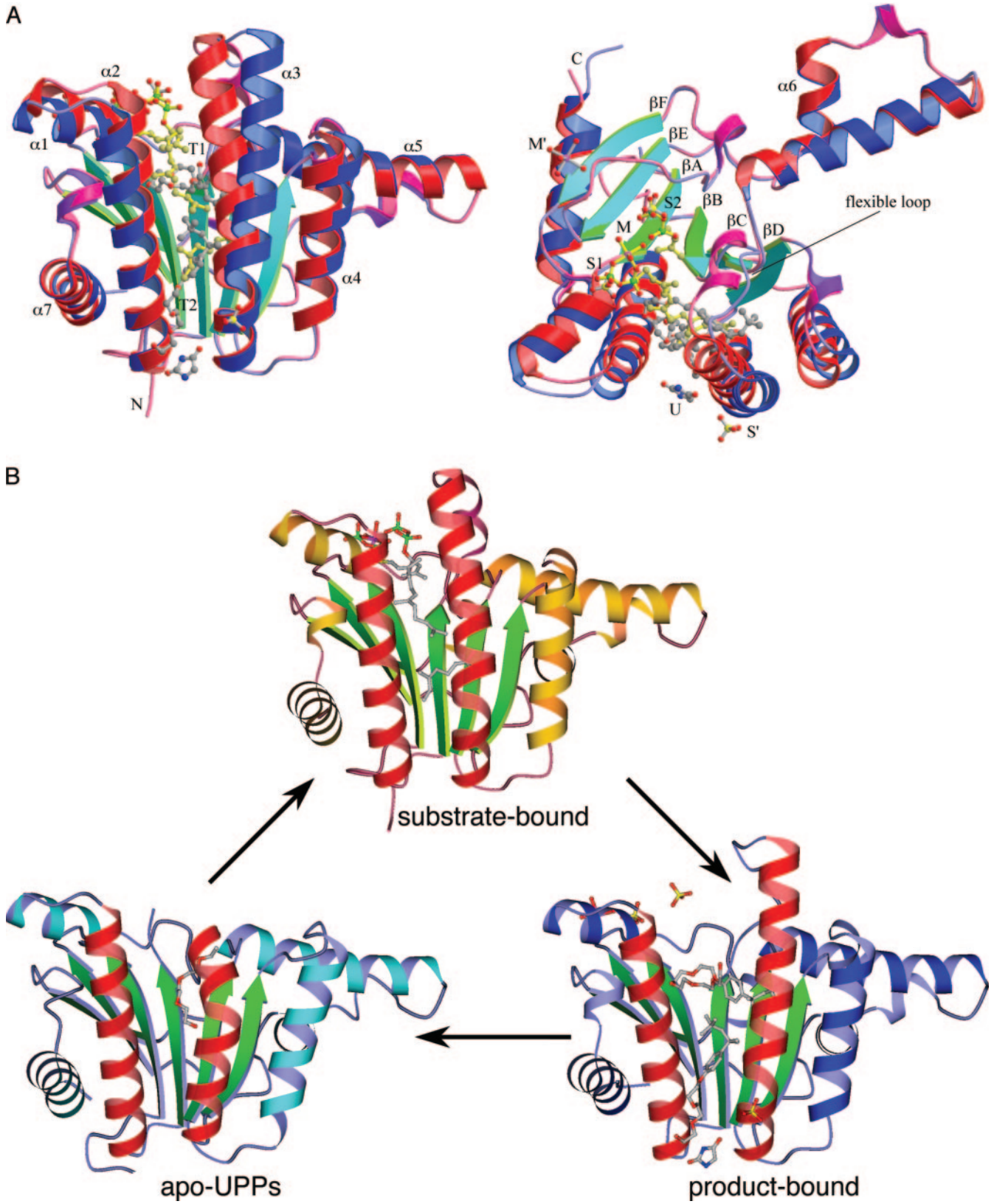

FIG. 2. **Overall fold of the protein.** *A*, the structure of UPPs in the WTF crystal is superimposed on that of Protein Data Bank 1UEH (B chain), which contains two bound Triton molecules. The UPPs monomers are viewed from two orthogonal directions. The α-helices, β-strands, and 3_{10} helices are shown in *red*, *green*, and *pink*, respectively, for the WTF structure, and those for the 1UEH are in *blue*, *cyan*, and *purple*. Helix α_3 is straight in the open conformation of 1UEH. In the closed conformation of WTF, it is kinked. The bound cofactors in 1UEH are shown with *gray bonds*, and those in WTF (and MTI) are in *yellow*. *S1* and *S2* refer to two previously defined pyrophosphate binding sites for the allylic and homoallylic substrates. The model of IPP bound to the S2 site is from the MTI structure. *T1* and *T2* are locations of two Triton molecules; *M* and *M'* are locations of Mg^{2+} in the active site and the allosteric site, respectively. *B*, three major conformations of UPPs are represented by the apoenzyme (*left*), the ternary complex with substrates and Mg^{2+} (*middle*), and another complex with Triton and sulfate (*right*). The helices α_2 and α_3 that flank the active site tunnel are *highlighted* in *red*, and the catalytic loop is highlighted in *magenta*. The apoenzyme with a PEG fragment in the tunnel has an intermediate conformation as compared with the closed substrate-bound and the open Triton-bound UPPs, but its catalytic loop is flexible and invisible.

confirmed. The first and the second Triton sites (T1 and T2 in Fig. 2*A*) are substituted by the hydrocarbon moieties of the bound FsPP molecules. In addition, a Mg^{2+} ion located between the two pyrophosphate groups of the substrates is seen in the active site (*M* in Fig. 2*A*). This new observation of the metal ion is distinct from the previous one (*M′*) at the dimer interface near strand βF and helix α_7, which is not observed here. The unknown cofactor U and a third sulfate (*S′*) near the C terminus of helix α_3, which are bound adjacent to the PEG tail of Triton T2, correspond to the pyrophosphate group of the second FPP molecule in the UPPs-FPP complex. In both orthorhombic and trigonal crystals, this region is involved in crystal contact with neighboring molecules. Due to disorders, no model can be built with certainty for the current crystal structures.

Structures of the Bound Substrate and Cofactors—The substrate binding sites of UPPs are all occupied in crystals of either the wild type or the mutant enzyme. In the WTF crystal, the entire FsPP molecule can be seen clearly, with an octahedrally coordinated Mg^{2+} ion bound to its pyrophosphate group. The Mg^{2+} ion is further coordinated to Asp^{26}. This represents the major difference compared with the UPPs-FPP structure in which the FPP is bound only through the hydrogen bonding and ionic interactions with the protein. However, densities for the IPP molecule are weak, which barely allow modeling of a phosphate group. As shown in Fig. 3*A*, the electron densities in the IPP binding site extend in three directions, indicating multiple conformations of the bound IPP in this crystal. On the other hand, inside the hydrophobic tunnel, there is another FsPP molecule bound to a similar position as the second (distal) FPP in the structure of UPPs-FPP (1V7U), but only a C_{10} geranyl moiety can be modeled (Fig. 3*B*). In the WTI crystal, similar dispositions of the pyrophosphates and Mg^{2+} are observed, but the isopentenyl group of IPP bound to the FPP site has a different arrangement than the farnesyl group of FsPP in the WTF crystal (Supplementary Fig. 2).

As shown in the above wild-type crystal structures, Asp^{26} uses its carboxylate side chain for chelation with the Mg^{2+}. Without the side chain carboxyl group of Asp^{26}, the pyrophosphate and Mg^{2+} ions are bound to the active site in a different manner. In the MTF crystal, a FsPP molecule and a C_{10} fragment of FsPP similar to that in the WTF crystal are seen. Densities are clear for the C_5 isopentenyl group of the bound IPP, but the pyrophosphate cannot be modeled with certainty, despite some corresponding densities (Supplementary Fig. 2). In the MTI crystal, two pyrophosphates are bound to the active site, with a bridging Mg^{2+}. The IPP bound to the S1 site is probably disordered, including the pyrophosphate group that may be shifted one step toward the Mg^{2+} ion, with the α-phosphate taking the β-position and the β-phosphate occupying the empty densities in Fig. 3*C*. The C_5 isopentenyl group of the second IPP seems to adopt two possible dispositions but is dominated by the one similar to that in the MTF crystal. The corresponding densities in the IPP binding site S2 are also seen in the WTF and WTI crystals (Fig. 3*A*; Supplemental Fig. 2). Although not all cofactors are completely modeled, an active site structure with both allylic and homoallylic substrates bound can be visualized with a composite model as shown in Fig. 3*D*. A number of positively charged arginine side chains bind to the substrate pyrophosphate groups, between which there is a Mg^{2+} ion coordinated to Asp^{26}. As will be discussed below, proximity of the hydrocarbon moieties makes the condensation reaction likely to occur.

The crystal structures of *E. coli* UPPs that contain bound substrate and substrate analogous molecules, solved previously and presently, are summarized in Table II. All of the cofactors bound to the catalytic site are superimposed in Fig. 4*A*, including those of the previous UPPs-FPP and UPPs-Triton complexes. In the WTF and WTI crystals, the pyrophosphate of FsPP or IPP is associated with the Mg^{2+} ion at the S1 site. Interestingly, the FsPP molecule appears to be somewhat distorted in the region of the first isoprene unit (C1–C5; Fig. 3*A*). In the MTF crystal, the FsPP does not show such distortion. Although the pyrophosphate of IPP at the S2 site is not well defined, the isopentenyl group is, as suggested by its low temperature factor (Table II). In the MTI crystal, the Mg^{2+} is not in direct contact with the S1 pyrophosphate but is associated with the IPP bound to the S2 site. As shown in Fig. 4*A*, the hydrocarbon moiety of the IPP in the MTI crystal is almost identical to that in the MTF crystal, suggesting a favored disposition of the properly bound isopentenyl group.

Interactions between the Enzyme and Substrates—In the previous structure of 1V7U, the pyrophosphate of FPP forms hydrogen bonds with the backbone nitrogen atoms of Gly^{29} and Arg^{30} as well as the side chains of Asn^{28}, Arg^{30}, and Arg^{39} (16). In the WTF crystal, the FsPP interacts with the enzyme via a similar but slightly different repertoire. As shown in Fig. 4*B*, the α-phosphate group makes two hydrogen bonds with the side chain of Arg^{77}, and so does the β-phosphate with Arg^{30}. The side chains of Asn^{28} and His^{43} bind, respectively, to the sulfur and oxygen atoms of the α-phosphate. Furthermore, the pyrophosphate group is coordinated with the bound Mg^{2+} ion, which is also coordinated by the side chain of Asp^{26} and three water molecules, forming an octahedral structure. The C_{15}-prenyl group of FsPP makes hydrophobic interactions with the surrounding side chains (not shown) of Met^{25}, Ala^{47}, Val^{50}, Ala^{69}, Leu^{85}, Leu^{88}, Phe^{89}, Ala^{92}, Ile^{141}, and Trp^{221} as well as the C_{10} fragment of the distal FsPP molecule. This C_{10} fragment makes additional hydrophobic interactions with the side chains of Val^{54}, Leu^{93}, Leu^{100}, Leu^{107}, and Leu^{139}. In the new conformation with bound Mg^{2+}, the C2 atom of FsPP hydrocarbon does not interact with the side chain of His^{43}, which is redirected toward the pyrophosphate instead. Although the C_5-prenyl group of IPP bound to the S1 site has a different arrangement in the WTI crystal, the pyrophosphate group makes virtually identical interactions with the enzyme and the metal ion.

In the MTF crystal, the bound FsPP molecule has a slightly different arrangement with the α-phosphate group rotated 120° with respect to the β-phosphate (Fig. 4*A*). The side chains of both Asn^{28} and His^{43} are hydrogen-bonded to the oxygen atoms of α-phosphate, leaving the S1 atom of FsPP alone, which is 3.6 Å away from the side chain of Arg^{77}. In addition, the α-phosphate is also hydrogen-bonded to the backbone nitrogen atom of Asn^{28} and possibly interacts with the nitrogen atom of Gly^{27} at a distance of 3.4 Å. These two backbone nitrogen atoms are 3.6–3.7 Å away from the S1 atom of FsPP in the WTF structure. Interactions of the farnesyl group with the hydrophobic tunnel and the distal geranyl fragment are similar to those in the WTF crystal. The isopentenyl group of IPP appears to be planar, although the single bond between C2 and C3 atoms allows free rotation. In both the MTF and MTI crystals, this group interacts with the side chain of Tyr^{68} at a distance of 3.4–3.7 Å, stabilizing the planar conformation (Fig. 3*D*). Detailed interactions of the IPP pyrophosphate with the UPPs active site residues in the MTI crystal are shown in Fig. 4*C*. The β-phosphate group makes hydrogen bonds to Arg^{194}, Arg^{200}, and Ser^{202} as the previous sulfate ion in the S2 site seen in the UPPs-Triton complex structure of 1UEH, and the α-phosphate group makes additional bonds to the side chains of Asn^{74} and Arg^{77}. These two residues are located in the catalytic loop of 72–82, which is visible only with both substrates bound to the enzyme. There is a Mg^{2+} ion coordinated to the IPP

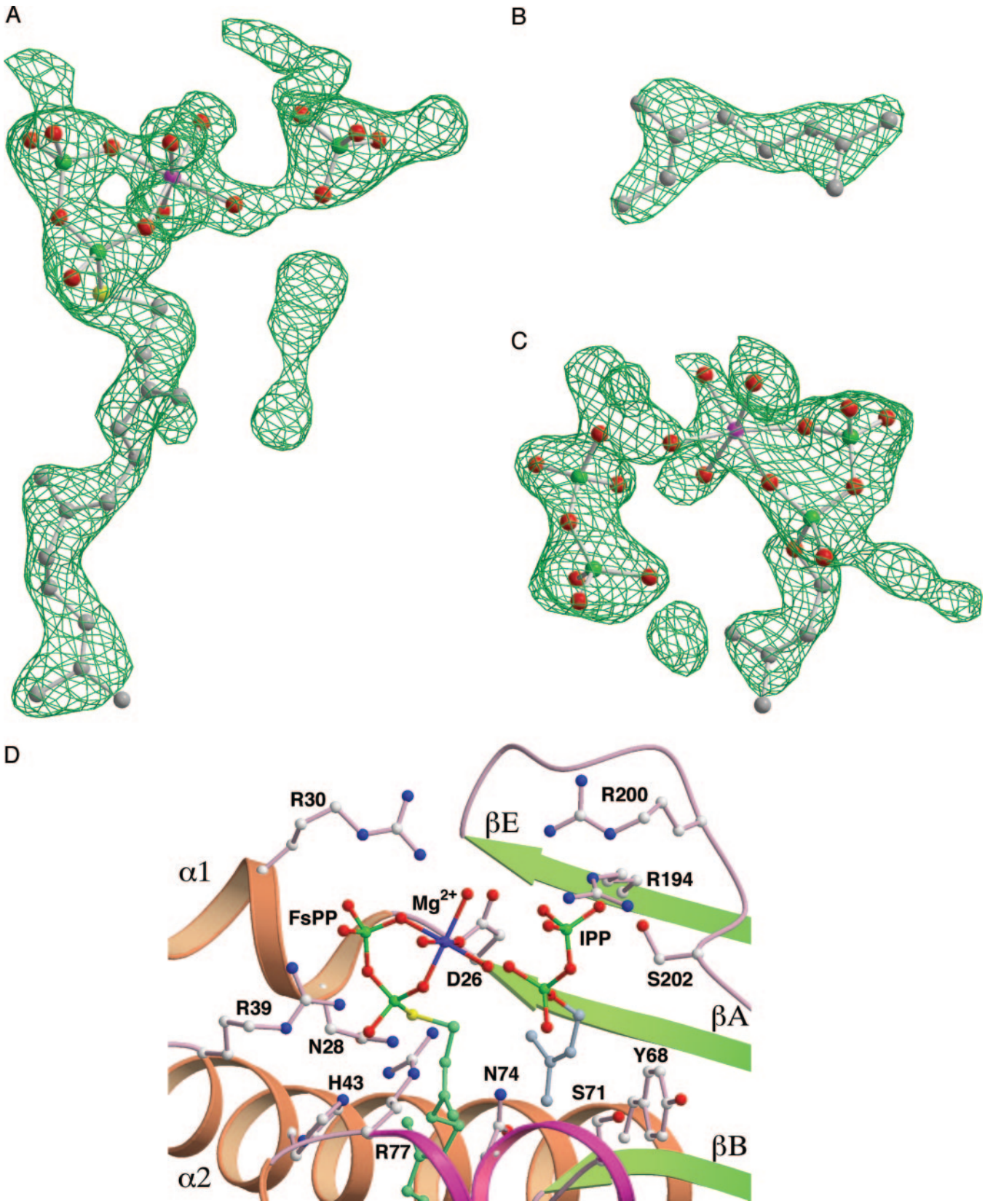

FIG. 3. **Substrate models in the active site of UPPs.** The $2F_o - F_c$ maps are contoured at 1.0 σ level and superimposed on the refined models of FsPP, Mg^{2+}, and a phosphate bound to the S1, M and S2 sites of UPPs in the WTF crystal (*A*), a fragment of FsPP bound to a distal site in the tunnel (*B*), and a pyrophosphate seen in the S1 site and an MgIPP complex in the M and S2 sites of UPPs in the MTI crystal (*C*). The carbon, oxygen, phosphorus, and sulfur atoms are *colored gray*, *red*, *green*, and *yellow*, respectively, whereas the Mg^{2+} ions are in *magenta*. The protein and solvent atoms are not shown, except those directly coordinated to Mg^{2+}. *D*, a composite model of UPPs with the Mg^{2+} and FsPP from the WTF crystal and the IPP from the MTI crystal. The amino acid side chains that interact with the Mg^{2+} and pyrophosphate ions are also shown.

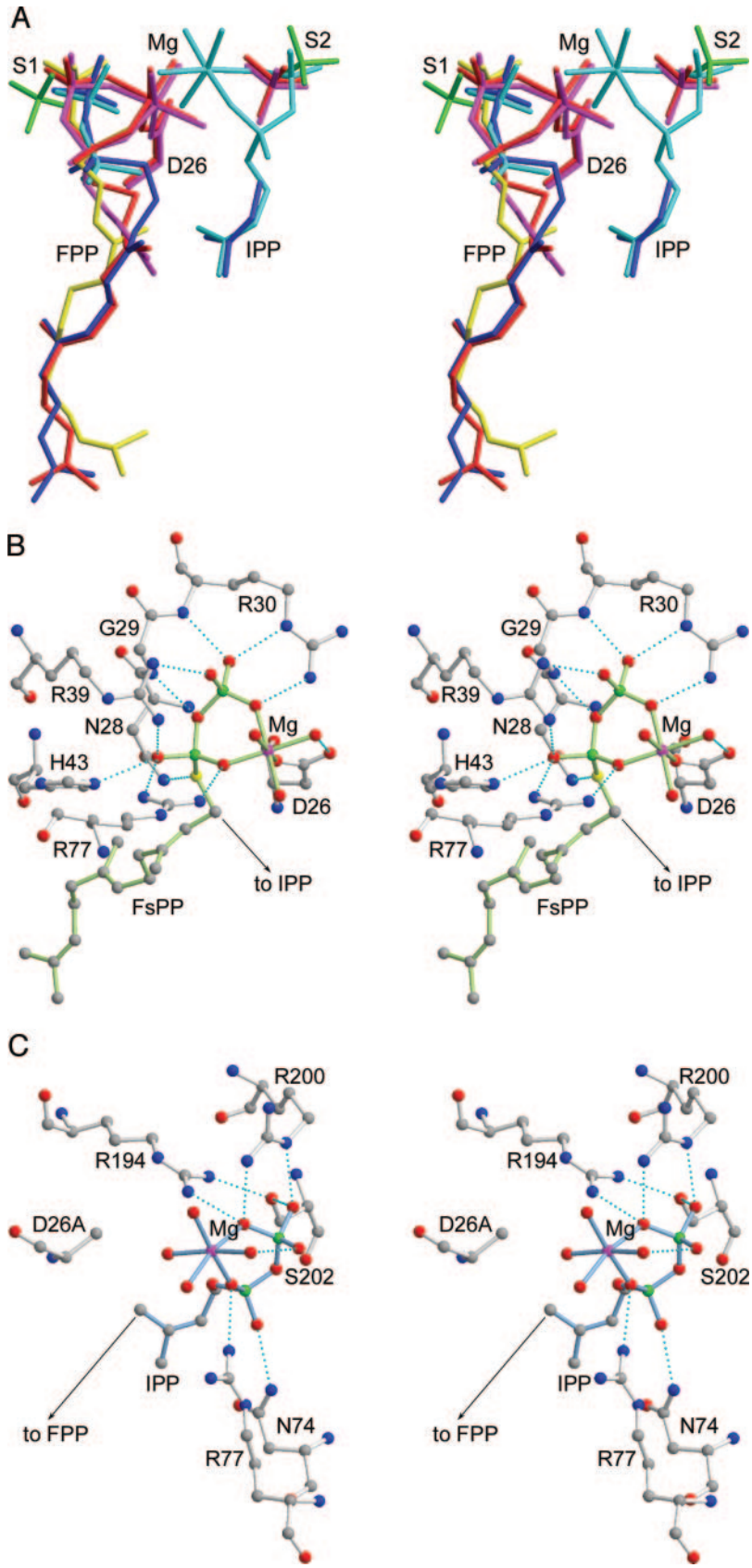

FIG. 4. **Substrate structures and interactions with UPPs.** *A*, the substrate and analogue molecules bound to the active site of UPPs are superimposed. The two sulfate ions S1 and S2 of Protein Data Bank structure 1UEH are shown in *green*, the FPP of 1V7U are in *yellow*, and those of the WTF, WTI, MTF, and MTI crystal structures studied here are in *red*, *magenta*, *blue*, and *cyan*, respectively. *B*, detailed interactions of the Mg^{2+} ion and the pyrophosphate moiety of the bound FsPP molecule with the UPPs protein in the WTF crystal. *C*, interactions of the bound MgIPP complex with the enzyme in the MTI crystal. Hydrogen bonds are shown as strings of small beads in cyan. The C1′ of FsPP and C4 of IPP in *B* and *C*, respectively, which form a new bond in the UPPs reaction, are labeled with *arrows*.

pyrophosphate. Because Asp^{26} has been mutated to alanine, the metal ion is not bound directly to the enzyme but to four water molecules.

Binding Mode Studied by Fluorescence Experiments—Since the complexed structures of UPPs are obtained from the crystal form of the enzyme saturated with high concentration of substrate (or analogue) and metal ion, methods that can distinguish the affinity of these ligands to the enzyme in solution are required to understand the substrate binding mode and the reaction mechanism. Both binding of FPP (or FsPP) and IPP to

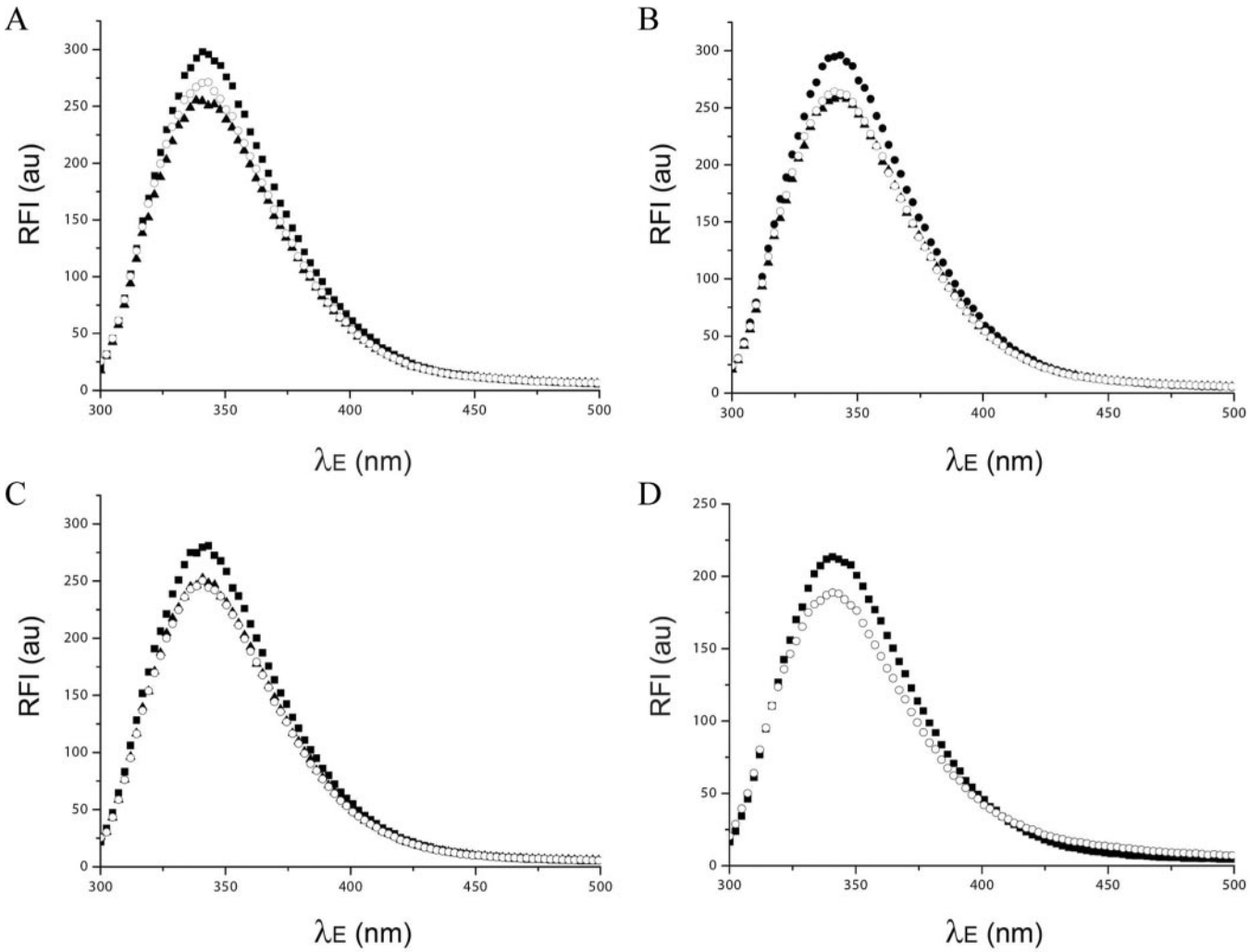

FIG. 5. **Fluorescence binding experiments by adding FsPP and IPP.** *A*, the intrinsic fluorescence of wild-type UPPs (1 μM) decreases upon the addition of FsPP (4 μM) and then increases by the addition of IPP (20 μM) in the presence of 1 mM Mg^{2+}. *au*, arbitrary units. *B*, with high concentration of Mg^{2+} (50 mM), the addition of IPP (20 μM) to the UPPs-FsPP complex does not change the protein fluorescence. *C*, for D26A UPPs mutant, the addition of FsPP still quenches the protein fluorescence, but the addition of IPP (20 μM) in the presence of Mg^{2+} (1 mM) fails to cause fluorescence change. The plots are drawn with *horizontal* and *vertical axes* representing the emission wavelength and the relative intensities, respectively. Shown are the fluorescence spectra of wild-type and D26A UPPs (■), spectra after the addition of FsPP (▲), and spectra after the further addition of IPP (○). *D*, protein intrinsic fluorescence changes of wild-type UPPs (1 μM) upon the addition of a high concentration of IPP (1 mM) in the absence of Mg^{2+} (a similar result was observed with 1 mM Mg^{2+}). Shown are the fluorescence spectrum of wild-type UPPs (■) and the spectrum after the addition of IPP (○). The same result was obtained for the D26A mutant.

UPPs give fluorescent signals that provide a way to measure the binding (16). As shown in Fig. 5*A*, the addition of FsPP (4 μM) quenches the intrinsic protein fluorescence and decrease of fluorescence is still observed in the absence of Mg^{2+} in solution, indicating that FsPP binding does not require the metal ion. The subsequent addition of IPP in the presence of FsPP and 1 mM Mg^{2+} increases the fluorescence, but not without Mg^{2+}. This indicates that in order for IPP to bind to UPPs, the Mg^{2+} is required. However, in the presence of a high concentration of Mg^{2+} (50 mM), the fluorescence change by adding IPP in the presence of FsPP was not observed, suggesting that excess Mg^{2+} inhibits the binding of MgIPP (Fig. 5*B*). In the D26A mutant where the Mg^{2+} binding is attenuated, FsPP (4 μM) still quenches the intrinsic fluorescence of UPPs (1 μM), but the further addition of IPP (20 μM) in the presence of 1 mM Mg^{2+} does not cause any change of the spectra (Fig. 5*C*). This indicates that Asp^{26} is important for IPP binding.

Adding IPP alone into UPPs solution causes fluorescence change only when a high concentration (1 mM) of IPP is employed, either with or without 1 mM Mg^{2+} (Fig. 5*D*), indicating weak binding of IPP to the FPP site. This is also consistent with the present crystal structure in which the IPP molecules occupy both the allylic and homoallylic sites when UPPs is co-crystallized with the high concentration of IPP alone. For D26A, similar results were obtained (not shown), also consistent with the structural data. Based on the above results, Mg^{2+} is not required for FPP binding. In the absence of Mg^{2+}, the pyrophosphate is bound to the S1 site of UPPs with a number of stabilizing interactions. However, Mg^{2+} is required for tight IPP binding. Consequently, the metal ion is essential for UPPs activity under physiological conditions where IPP concentration is lower.

Reaction Kinetics with Different Concentrations of Mg^{2+}—From the above results, the binding of IPP requires Mg^{2+}, but too high [Mg^{2+}] (50 mM) inhibits the binding, so we further investigate the [Mg^{2+}] effect on enzyme activity. The measurement for [Mg^{2+}] dependence of the IPP condensation rate catalyzed by UPPs in Fig. 6*A* shows that the enzyme activity increases with the concentration of Mg^{2+} from 0.02 to 1 mM and then declines significantly when the concentration is at 50 mM. The CD spectra of UPPs in the presence or absence of 5 mM $MgCl_2$ are similar, and the estimated T_m value is 55 °C in

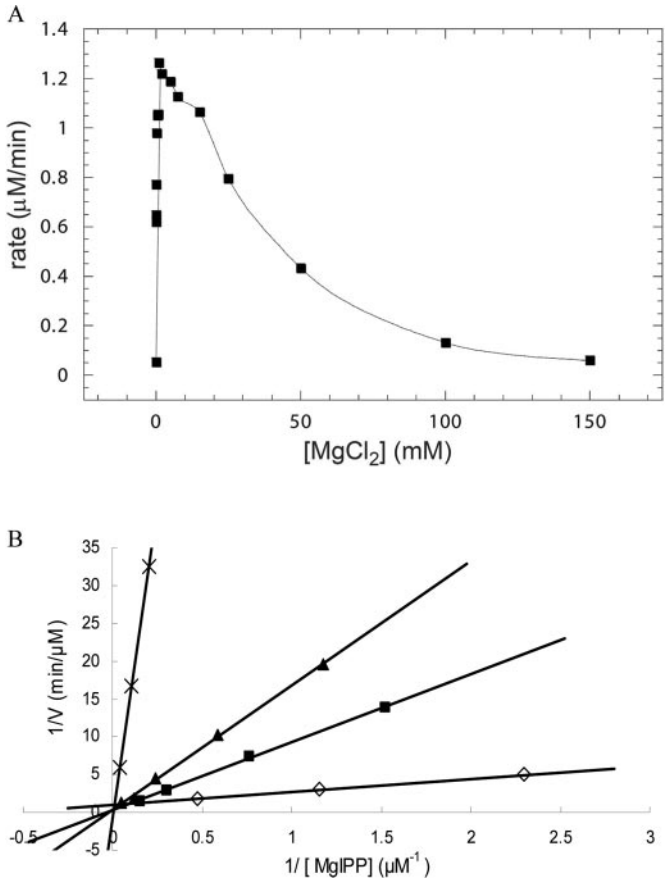

FIG. 6. **Effects of Mg^{2+} ion on the UPPs activity.** *A*, Mg^{2+} concentration dependence of [^{14}C]IPP incorporation rate by UPPs. The enzyme activity based on the rate of IPP incorporation was measured at different [Mg^{2+}] from 0.02 to 150 mM. The UPPs activity increases with increased [Mg^{2+}], reaching the maximum approximately at [Mg^{2+}] = 1 mM, and then drops. *B*, measurements of the Mg^{2+} inhibition constant when Mg^{2+} is in excess. The activity of a reaction mixture containing UPPs (0.01 μM), FPP (5 μM), Mg^{2+} (0.05, 1, 3, or 50 mM), and a varied concentration of [^{14}C]IPP was measured. The [MgIPP] was calculated from the [IPP] and [Mg^{2+}] in solution using the reported $K_{d(MgIPP)}$ = 520 μM. The competitive inhibition constant K_i was determined to be 1.1 ± 0.4 mM.

either situation, indicating that Mg^{2+} is not required for overall structure stability.[2] The activity-enhancing effect of Mg^{2+} at low concentration on UPPs is probably due to formation of the MgIPP complex, an active substrate species with K_d = 520 μM, in solution before binding to the enzyme. When [Mg^{2+}] is further increased and the free metal ion begins to bind to the active site, it becomes a competitive inhibitor with respect to MgIPP. The K_i value of Mg^{2+} derived from the inhibition data shown in Fig. 6*B* is 1.1 ± 0.4 mM. The K_m value of IPP also varies with the Mg^{2+} concentration. As summarized in Table III, at 50 mM Mg^{2+}, where binding of the MgIPP complex to the enzyme is inhibited, the IPP K_m value becomes 291 μM, remarkably larger than that (4 μM) measured at 0.5 mM Mg^{2+}. The k_{cat} value cannot be measured accurately with such a large IPP K_m value. At lower Mg^{2+} concentration, the kinetic parameters are not significantly different.

Kinetic Parameters of the Mutants—In a previous study of the UPPs mutant D26A, we showed that the enzymatic activity is reduced about 1000-fold with the removal of the side-chain carboxyl group of Asp^{26} (24). Because the crystallographic, spectroscopic and kinetic results presented above suggest the vital importance of this residue in binding the Mg^{2+} ion and catalysis, we further substitute it with glutamate, lysine, and arginine residues by producing the site-specific mutants D26E, D26K, and D26R, respectively, purify them, and measure their k_{cat} and K_m. The results are also summarized in Table III. All of these three new mutants, like the foregoing mutant of D26A, lose the enzyme activity to even a greater extent than simple removal of the side chain. The additional methylene group in the side chain of Glu^{26} is likely to deprive the enzyme of the optimal geometry for binding the Mg^{2+} ion, which should also coordinate with the substrate pyrophosphate. The positively charged side chains of Lys^{26} or Arg^{26} in the other two mutants are supposed to offer electrostatic force to assist the ionization of pyrophosphate from FPP. However, the results also turn out to be inactivation.

Interestingly, as shown in Table III, the K_m for the allylic substrate FPP is affected to a much smaller extent, if at all, by the mutations at Asp^{26}. These low K_m values are consistent with the results of fluorescence studies, suggesting that binding of FPP does not require Mg^{2+} and does not involve the side chain of Asp^{26}. Instead, UPPs interacts with the allylic substrate principally via the structural P-loop near the N-terminal end of helix α_1 and its associated positively charged residues. In a previous mutagenesis study of *Micrococcus luteus* UPPs (35), it was shown that the double mutant of G32R/R42G (corresponding to Gly^{29} and Arg^{39} in *E. coli* UPPs; Fig. 1) retained original activity and product characteristics of the enzyme, manifesting the importance of the complementarily conserved arginines in catalysis. On the other hand, the K_m values of the mutants at Asp^{26} for IPP show a significant 2–5-fold increase, indicating the interactions of Asp^{26} with Mg^{2+} are probably responsible for IPP binding and other concerted rearrangements of the substrate molecules and active site structure for efficient catalysis. Neither the side chain of Asp^{26} nor the Mg^{2+} ion can be substituted by the side chains of glutamate, lysine, or arginine without loss of their optimized functionality.

DISCUSSION

Role of the Metal Ion in UPPs Catalysis—In conjunction with the previous studies (16, 21), our fluorescence data presented here show that the allylic substrate FPP can bind to UPPs without Mg^{2+}, but binding of the homoallylic substrate IPP requires Mg^{2+}. Since $K_{d(MgIPP)}$ = 520 μM, a sufficient amount of Mg^{2+} (1 mM) with 20 μM IPP as used in the experiments is required to form MgIPP in solution for optimal activity. It has been demonstrated that FPP binds first to UPPs (21). The MgIPP is then bound to the active site to trigger the condensation reaction. Without bound IPP, the UPPs-FPP complex has lower affinity for Mg^{2+}, consistent with the absence of Mg^{2+} in the active site of the crystal structure of UPPs-FPP complex (16). Because the addition of MgIPP to the UPPs-FPP complex will lead to the formation of product, in this study, the almost inactive thiol analogue of FsPP was used to prepare a ternary complex for structural studies. This strategy turns out to be effective in elucidating the interactions of Mg^{2+} with the enzyme and the substrates and giving the new mechanistic information, particularly the role of metal ion in catalysis, as presented in this study. Mg^{2+} may not be required for FPP binding but is associated with the pyrophosphate of FPP in the ternary complex and essential for the UPPs reaction by facilitating the pyrophosphate elimination (see below). IPP is bound to the S2 site and is also coordinated to Mg^{2+}. An excess of Mg^{2+} seems to occupy the metal binding site adjacent to Asp^{26}, seen in the WTF and WTI structures, and inhibits further binding of MgIPP. As shown in the [Mg^{2+}] dependence of the IPP condensation rate, the UPPs activity reaches the peak value at 1 mM [Mg^{2+}] and drops significantly at [Mg^{2+}] = 50 mM. At high concentration, the metal ion inhibits the reaction

[2] A. P.-C. Chen and P. H. Liang, unpublished data.

TABLE III
Kinetic parameters of the wild-type and mutant E. coli UPPs in various concentrations of $MgCl_2$

	k_{cat}	$K_{m(FPP)}$	$K_{m(IPP)}$	Relative k_{cat}[a]
	s^{-1}	μM	μM	
Wild type				
0.05 mM $MgCl_2$	1.23 ± 0.1	1.5 ± 0.1	11.5 ± 2	0.49
0.5 mM $MgCl_2$[b]	2.5 ± 0.1	0.4 ± 0.1	4.1 ± 0.3	1
1 mM $MgCl_2$	1.98 ± 0.18	0.37 ± 0.07	9.7 ± 2.3	0.800
3 mM $MgCl_2$	1.92 ± 0.18	0.44 ± 0.05	17.5 ± 3.2	0.775
50 mM $MgCl_2$		1.57 ± 0.1	291 ± 36	
Mutants ([$MgCl_2$] = 0.5 mM)				
D26A[b]	3.3×10^{-3}	0.5 ± 0.1	14.1 ± 1.4	1.3×10^{-3}
D26E	3.66×10^{-4}	0.67 ± 0.09	20.8 ± 2.6	1.5×10^{-4}
D26K	7.66×10^{-5}	0.46 ± 0.12	9.2 ± 3.3	3.1×10^{-5}
D26R	6.33×10^{-5}	0.55 ± 0.01	22.3 ± 3.0	2.5×10^{-5}
S71A[b]	0.11	1.0 ± 0.2	133 ± 14	4×10^{-2}
N74A[b]	2.20×10^{-2}	0.4 ± 0.1	8 ± 0.6	1×10^{-2}
R77A[b]	1.4×10^{-4}	1.6 ± 0.3	15.7 ± 2.5	5×10^{-3}

[a] k_{cat} relative to that of the wild type enzyme.
[b] Data taken from Refs. 14 and 24.

with K_i = 1 mM competitively with respect to MgIPP, and the IPP K_m value becomes significantly larger.

Our data presented here are consistent with a recent study that concluded that a metal ion such as Mg^{2+} or Mn^{2+} acts as a regulatory factor to control the enzyme activity and product chain length of the *cis*-type rubber prenyltransferase (36). This enzyme catalyzes the condensation of thousands IPP molecules with an initiator FPP to form natural rubber. The metal ion is required for rubber biosynthesis, but an excess of the metal ion inhibits its activity (36). However, the kinetic characteristic of purified UPPs is somewhat different from that of the rubber prenyltransferase in the washed rubber particles from *Hevea brasiliensis*. When [Mg^{2+}] is increased from 4 to 8 mM, the K_m of MgIPP for rubber prenyltransferase decreases from 8000 to 68 μM, reflecting a large increase in affinity that the authors believe is due to a conformational change caused by binding of free Mg^{2+} to an allosteric site in the enzyme that either is or affects an activator site (36). In the case of UPPs, 4 or 8 mM Mg^{2+} makes little difference in the kinetic parameters. The allosteric role of Mg^{2+} as suggested in the rubber prenyltransferase is not clear in UPPs. However, In Fig. 6*A*, there is a lag in the activity drop near [Mg^{2+}] = 10 mM, implying a third component other than IPP binding and competitive inhibition that contributes to the Mg^{2+} dependence of UPPs activity. A Mg^{2+} has been observed previously at the dimer interface near the C terminus of the counter monomer, which contains a number of positively charged residues that may interact with IPP (15). It was not observed in the 1V7U structure, probably due to the low [Mg^{2+}] of 0.5 mM employed; nor is it seen in the structures presented here, because all free Mg^{2+} has probably been depleted by IPP (both 2.5 mM) in the crystallization solution. The poor affinity of UPPs with the metal ion in the absence of the substrate classifies the *cis*-prenyl transferase as a metal-activated enzyme using Mg^{2+} rather than a metalloenzyme to which a metal ion is tightly bound.

The binding mode of UPPs is further supported by the results of fluorescence binding experiments. We have shown that without Mg^{2+}, the fluorescence change of adding FsPP (4 μM) can still be observed, but adding IPP (20 μM) does not cause the further change of fluorescence, indicating that FPP binding does not require Mg^{2+} but IPP binding does. Furthermore, we show in the fluorescence study that high concentration (50 mM) of Mg^{2+} inhibits the binding of MgIPP to the enzyme, consistent with the kinetic data. In the crystal structures of WTI and MTI, we also observe that without FsPP, a large amount of IPP (2.5 mM) seems to promote its binding to both the allylic and homoallylic sites. It is likely that the tight IPP binding to the S2 site requires Mg^{2+}, which also requires a bound FPP at the S1 site to proceed with the condensation reaction, whereas loose IPP binding to the S1 site does not.

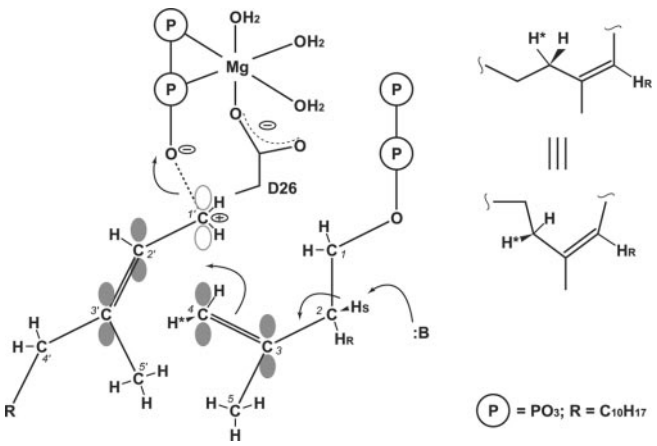

SCHEME 1. **Stereochemistry of UPPs reaction.**

Stereochemistry of the UPPs Reaction and Proposed Catalytic Mechanism—The crystal structure of the UPPs-FPP complex does not contain Mg^{2+}, in which the conformation of bound FPP also differs from those of the FsPP bound to the WTF and MTF crystals by an approximately ±120° rotation of the α-phosphate group, which forms only a hydrogen bond with the side chain of Asn^{28} in 1V7U. The O1 atom in this conformation does not allow formation of three hydrogen bonds with the side chains of Arg^{39}, His^{43}, and Arg^{77} as observed in the WTF crystal. On the other hand, the different orientations of the pyrophosphate group bound to the S1 site in the wild type and mutant UPPs structures can be linked, respectively, to the properly bound and less optimally bound Mg^{2+} ion to the active site. Specifically, Mg^{2+} does not interact with the S1 or O1 atom of FsPP or IPP bound to the S1 site when it is directly bound to Asp^{26}, but it has to interact with an oxygen atom of the α-phosphate group. Therefore, the optimal conformation of bound FPP should be similar to FsPP in the WTF crystal. However, the geometry tends to be distorted in this conformation, whereas the S1 atom of FsPP (equivalent to O1 of FPP) forms a hydrogen bond to the side chain of Asn^{28} and may further interact with the backbone nitrogen atoms of Gly^{27} and Asn^{28}. It is likely that these two nitrogen atoms play a role similar to the oxyanion hole in other enzymes, including serine proteases, to accommodate the negative charge developed in the transition states. Consequently, it seems reasonable to believe that the bound FPP changes from the conformation in 1V7U to the conformation in WTF upon binding of IPP and Mg^{2+} via the

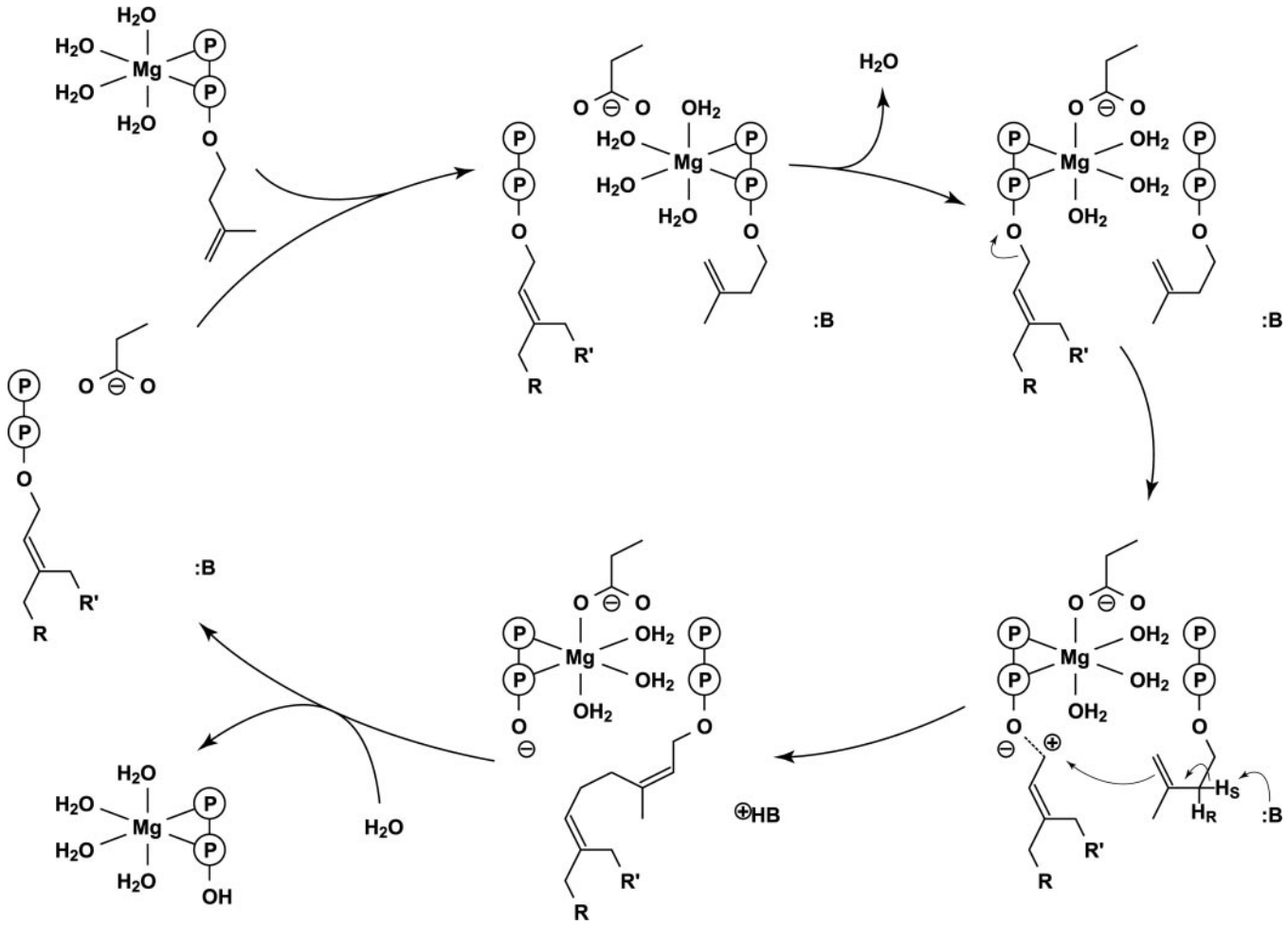

SCHEME 2. **Catalytic mechanism of UPPs.**

conformation in MTF. This is probably driven by synergic movements of the loop of 72–82 and the helices α_1, α_2, and α_3, which host the essential amino acid residues for catalysis.

In Fig. 4*A*, the distances between the C1′ atom of FsPP and the C4 atom of IPP are 3.0–3.6 Å, whereas those between FsPP C1′ and IPP C5 are 3.9–4.7 Å. Because the C4 assumes a *cis*-like position about the C2–C3 bond, relative to the C1 of the bound IPP as seen in the MTF and MTI structures, the attack of IPP C4 on FPP C1′ will result in the formation of a new *cis*-double bond of C2-C3, consistent with the stereochemistry of the UPPs-catalyzed reaction. As shown in Scheme 1, distortion in the bound FPP as a result of the coordination of its oxygen atoms to the Mg^{2+} ion destabilizes the O1–C1′ bond, where the negative charged developed on the O1 atom is compensated by the metal ion, the N-terminal dipole of helix α_2, the positively charged side chains, and backbone nitrogen atoms. The positive charge developed on C1′ of FPP is compensated by delocalization of the π-electrons on C2′ and C3′. This partially positively charged character on C2′ of the allylic substrate is shared by FPP synthase, because the fluoro-substituted geranyl pyrophosphate analogue is a poor substrate for FPP synthase due to fluorine's strong electronegativity to destabilize the intermediate (17). On the other hand, upon subtraction of the H_S atom on C2 of IPP by some base, the C2 atom becomes negatively charged and transforms to a planar configuration. The π-electrons on C2 then contribute to the new double bond formed between C2 and C3, and a new single bond is formed by linking the C4 of IPP and the C1′ of the farnesyl group of FPP, whereas the O1–C1′ bond is broken. The stereochemistry of *cis*-prenyltransferases has been studied extensively (reviewed in Refs. 3 and 4). The mechanism proposed in Scheme 1 is fully consistent with the known stereochemistry, including the H_R and H_S on C2 and the H and H* on C4 of IPP. It is not clear, however, whether the reaction proceeds by an ionization condensation elimination mechanism as for the *trans*-prenyltransferases in which a C1′ carbonium of FPP is formed first or by an SN2-like concerted mechanism where the extraction of proton on the C2 of IPP initiates the reaction.

Based on the x-ray structural data as well as the fluorescence binding and [Mg^{2+}] dependence of enzyme activity, a plausible mechanism of UPPs reaction is outlined in Scheme 2. FPP binds to the S1 site of the enzyme first, and the enzyme-substrate interactions are initially stabilized by Asn^{28}, Gly^{29}, Arg^{30}, Arg^{39}, and His^{43} to provide hydrogen bonding and electrostatic interactions for the pyrophosphate of FPP and the hydrophobic amino acids for the C_{15}-prenyl tail. These interactions lead to change of UPPs from the open to the closed conformation, in which the originally flexible loop turns into an ordered structure. The MgIPP complex then binds to the S2 site. The carboxyl group of Asp^{26} assists the migration of Mg^{2+} from IPP to FPP. The importance of Asp^{26} in catalysis has been revealed by the 1000-fold reduction in the k_{cat} value of D26A mutant (24). It cannot be replaced by other charged amino acids. Without Asp^{26}, the Mg^{2+} remains bound to IPP. The pyrophosphate group can leave the FPP only when facilitated by the bound Mg^{2+}. His^{43} is involved in binding FPP and may also serve as a proton donor. Because the complete reaction results in the net transfer of a proton from C2 of IPP to the pyrophosphate of FPP over a long distance, it must involve solvent molecules. Protonation of the pyrophosphate may be

contributed by solvent molecule as well. However, the reaction is much slower without His^{43} as a temporary proton carrier. The mutation of H43A causes the decrease of k_{cat} value by 1000-fold, suggesting its importance in catalysis (15).

Regarding the general base to remove a proton from IPP, a possible candidate is Asn^{74}, of which the ND2 atom is hydrogen-bonded to the pyrophosphate and the OD1 atom is close to the C2 atom of IPP. Another candidate is Ser^{71} (Fig. 3*D*). If the side chain of Ser^{71} is rotated 120°, to a favored conformation, its OG atom will interpolate between the OD1 of Asn^{74} and the C2 of IPP, which constitutes a proton relay. Judging from the MTF and MTI structures (Figs. 3*D* and 4*C*), the H_R atom of IPP C2 in Scheme 1 should be directed toward the interior of the active site and the H_S atom facing the outside. Therefore, the proton may be subtracted directly by the solvent as well, but better with Ser^{71} and Asn^{74} serving temporary roles of proton acceptor. After each elongation step, the original pyrophosphate group of IPP migrates from the S2 site to the S1 site, probably assisted by the positively charged side chain of Arg^{77}, which can alternately interact with the pyrophosphate of either FPP or IPP. The hydrocarbon in Scheme 2 also switches from R to R′ after the first cycle of reaction, because the new double bond is in *cis*-configuration. The kinetic data for S71A, N74A, and R77A reported previously (14, 24) (Table III) show significantly reduced k_{cat} values and a particularly high K_m for S71A, indicating the importance of these conserved amino acids in the catalysis by UPPs.

Acknowledgments—We thank Dr. Shuenn-Shing Chern, You-Liang Cheng, and Ya-Shan Cheng for technical assistance. This work is based upon research conducted at the National Synchrotron Radiation Research Center, Taiwan, using the Biological Crystallography Facility at NSRRC (BioNSRRC).

REFERENCES

1. Kellogg, B. A., and Poulter, C. D. (1997) *Curr. Opin. Chem. Biol.* **1,** 570–578
2. Ogura, K., Koyama, T., and Sagami, H. (1997) *Subcell. Biochem.* **28,** 57–88
3. Ogura, K., and Koyama, T. (1998) *Chem. Rev.* **98,** 1263–1276
4. Liang, P. H., Ko, T. P., and Wang, A. H.-J. (2002) *Eur. J. Biochem.* **269,** 3339–3354
5. Asai, K.-I., Fujisaki, S., Nishimura, Y., Nishino, T., Okada, K., Nakagawa, T., Kawamukai, M., and Matsuda, H. (1994) *Biochem. Biophys. Res. Commun.* **202,** 340–345
6. Pan, J. J., Kuo, T. H., Chen, Y. K., Yang, L. W., and Liang, P. H. (2002) *Biochim. Biophys. Acta* **1594,** 64–73
7. Allen, C. M. (1985) *Methods Enzymol.* **110,** 281–299
8. Robyt, J. (1998) in *Essentials of Carbohydrate Chemistry*, pp. 305–318, Springer-Verlag, New York
9. Shimizu, N., Koyama, T., and Ogura, K. (1998) *J. Biol. Chem.* **273,** 19476–19481
10. Apfel, C. M., Takacs, B., Fountoulakis, M., Stieger, M., and Keck, W. (1999) *J. Bacteriol.* **181,** 483–492
11. Guo, R. T., Kuo, C. J., Chou, C. C., Ko, T. P., Shr, H. L., Liang, P. H., and Wang, A. H.-J. (2004) *J. Biol. Chem.* **279,** 4903–4912
12. Guo, R. T., Kuo, C. J., Ko, T. P., Chou, C. C., Liang, P. H., and Wang, A. H.-J. (2004) *Biochemistry* **43,** 7678–7686
13. Fujihashi, M., Zhang, Y.-W., Higuchi, Y., Li, X.-Y., Koyama, T., and Miki, K. (2001) *Proc. Natl. Acad. Sci. U. S. A.* **98,** 4337–4342
14. Ko, T. P., Chen, Y. K., Robinson, H., Tsai, P. C., Gao, Y.-G., Chen, A. P.-C., Wang, A. H.-J., and Liang, P. H. (2001) *J. Biol. Chem.* **276,** 47474–47482
15. Chang, S. Y., Ko, T. P., Liang, P. H., and Wang, A. H.-J. (2003) *J. Biol. Chem.* **278,** 29298–29307
16. Chang, S. Y., Ko, T. P., Chen, A. P.-C., Wang, A. H.-J., and Liang, P. H. (2004) *Protein Sci.* **13,** 971–978
17. Poulter, C. D., Argyle, J. C., and Mash, E. A. (1977) *J. Am. Chem. Soc.* **99,** 957–959
18. Joly, A., and Edwards, P. A. (1993) J. *Biol. Chem.* **268,** 26983–26989
19. Chen, A., Kroon, P. A., and Poulter, C. D. (1994) *Protein Sci.* **3,** 600–607
20. Hosfield, D. J., Zhang, Y., Dougan, D. R., Broun, A., Tari, L. W., Swanson, R. V., and Finn, J. (2004) *J. Biol. Chem.* **279,** 8526–8529
21. Chen, Y. H., Chen, A. P., Chen, C. T., Wang, A. H.-J., and Liang, P. H. (2002) *J. Biol. Chem.* **277,** 7369–7376
22. Chang, S. Y., Chen, Y. K., Wang, A. H.-J., and Liang, P. H. (2003) *Biochemistry* **42,** 14452–14459
23. Pan, J. J., Chiou, S. T., and Liang, P. H. (2000) *Biochemistry* **39,** 10936–10942
24. Pan, J. J., Yang, L. W., and Liang, P. H. (2000) *Biochemistry* **39,** 13856–13861
25. Otwinowski, Z., and Minor, W. (1997) *Methods Enzymol.* **276,** 307–326
26. Brunger, A. T. (1993) *Acta Crystallogr. Sect. D Biol. Crystallogr.* **49,** 24–36
27. Brunger, A. T., Adams, P. D., Clore, G. M., DeLano, W. L., Gros, P., GrosseKunstleve, R. W., Jiang, J.-S., Kuszewski, J., Nilges, M., Pannu, N. S., Read, R. J., Rice, L. M., Simonson, T., and Warren, G. L. (1998) *Acta Crystallogr. Sect. D Biol. Crystallogr.* **54,** 905–921
28. Jones, T. A., Zou, J. Y., Cowan, S. W., and Kjeldgaard, M. (1991) *Acta Crystallogr. Sect. A* **47,** 392–400
29. Barton, G. J. (1993) *Protein Eng.* **6,** 37–40
30. Kraulis, P. J. (1991) *J. Appl. Crystallogr.* **24,** 946–950
31. Esnouf, R. M. (1997) *J. Mol. Graph.* **15,** 132–134
32. Merrit, E. A., and Murphy, M. E. P. (1994) *Acta Crystallogr. Sect. D Biol. Crystallogr.* **50,** 869–873
33. King, H. L., and Rilling, H. C. (1977) *Biocehmistry* **16,** 3815–3819
34. Chen, A. P.-C., Chang, S. Y., Lin, Y. C., Sun, Y. S., Chen, C. T., Wang, A. H.-J., and Liang, P. H. (2005) *Biochem. J.* **386,** 169–176
35. Fujikura, K., Zhang, W.-Y., Fujihashi, M., Miki, K., and Koyama, T (2003) *Biochemistry* **42,** 4035–4041
36. da Costa, B. M. T., Keasling, J. D., and Cornish, K. (2005) *Macromolecules* **6,** 279–289